Doped semiconductor nanocrystal junctions

Lukasz Borowik, Thuat Nguyen-Tran, Pere Roca I Cabarrocas, Thierry Melin

Doped semiconductor nanocrystal junctions

Cite as: J. Appl. Phys. **114**, 204305 (2013); https://doi.org/10.1063/1.4834516
Submitted: 15 September 2013 • Accepted: 31 October 2013 • Published Online: 27 November 2013

Ł. Borowik, T. Nguyen-Tran, P. Roca i Cabarrocas, et al.

Doped semiconductor nanocrystal junctions

Ł. Borowik,[1] T. Nguyen-Tran,[2] P. Roca i Cabarrocas,[2] and T. Mélin[1,a)]
[1]*Institut d'Electronique, de Microélectronique et de Nanotechnologie, CNRS-UMR8520, Avenue Poincaré, F-59652 Villeneuve d'Ascq, France*
[2]*Laboratoire de Physique des Interfaces et des Couches Minces, CNRS-UMR7647, Ecole Polytechnique, F-91128 Palaiseau, France*

(Received 15 September 2013; accepted 31 October 2013; published online 27 November 2013)

Semiconductor junctions are the basis of electronic and photovoltaic devices. Here, we investigate junctions formed from highly doped ($N_D \approx 10^{20} - 10^{21}\,\mathrm{cm}^{-3}$) silicon nanocrystals (NCs) in the 2–50 nm size range, using Kelvin probe force microscopy experiments with single charge sensitivity. We show that the charge transfer from doped NCs towards a two-dimensional layer experimentally follows a simple phenomenological law, corresponding to formation of an interface dipole linearly increasing with the NC diameter. This feature leads to analytically predictable junction properties down to quantum size regimes: NC depletion width independent of the NC size and varying as $N_D^{-1/3}$, and depleted charge linearly increasing with the NC diameter and varying as $N_D^{1/3}$. We thus establish a "nanocrystal counterpart" of conventional semiconductor planar junctions, here however valid in regimes of strong electrostatic and quantum confinements. © *2013 AIP Publishing LLC*. [http://dx.doi.org/10.1063/1.4834516]

I. INTRODUCTION

Semiconductor junctions are building bocks for micro and nanoelectronics and are essential elements for charge separation—and thus the efficiency—of photovoltaic devices. A natural pathway for future applications may consist in replacing traditional doped semiconductor layers by functional self-assemblies of doped nanocrystals (NCs),[1–3] with obvious advantages to build flexible electronic and/or photovoltaic devices.[4,5] This raises the issue of the understanding semiconductor junctions based on doped NCs as a function of the semiconductor doping level N_D: charge transfer, depletion width, or built-in electric field. Such an understanding has not been achieved so far, for two main reasons. On one hand, because quantum and electrostatic confinements are highly enhanced in NCs and easily exceed bulk material bandgaps,[6] which turns the understanding of charge transfers from doped NCs into a complex issue. On the other hand, the synthesis itself of doped NCs has remained quite difficult.[7,8] It is now subject to intense studies, and available for a few colloidal materials[1–4,9,10] as well as for traditional semiconductor nanomaterials.[11–13]

In this Article, we solve the issue of understanding doped semiconductor NC junctions by measuring charge transfers from doped NCs from scanning probe microscopy experiments. From a detailed analysis of experiments, we propose an original simple analytical description of doped NC junction depletion properties down to quantum size regime. This description is a "nanocrystal counterpart" of traditional semiconductor junction physics.

To do so, we start from the measurement of the ionization state of individual doped NCs by Kelvin Probe Force Microscopy (KPFM) with single charge sensitivity, at 300 K. Such experiments have already enabled to measure NC quantum confinement effects.[14] Doped NC junction properties are investigated under a randomly distributed impurity model and for doping levels N_D in the range $N_D \approx 10^{20}$–$10^{21}\,\mathrm{cm}^{-3}$. We observe experimentally that in spite of electrostatic and quantum confinement, doped NC junctions simply form an interface dipole linearly increasing with the NC diameter, and equal to ≈15 Debye for a 1 nm diameter NC. This feature leads to analytically predictable junction width W scaling as $N_D^{-1/3}$ (independent of the NC size) and junction depletion charge Q_{dep} scaling as $N_D^{1/3}$ and proportional to the NC diameter. The predictions for W and Q_{dep} agree with experiments in a 2–50 nm NC size range. Charge transfers from doped NCs can thus be predicted analytically down to quantum size regimes.

II. EXPERIMENTAL DETAILS

Doped silicon nanocrystals have been fabricated by plasma enhanced chemical vapor deposition using silane (SiH_4) as silicon source, and phosphine (PH_3) as phosphorus source for *n*-type doping.[13] They have been deposited on *n*-type silicon substrates with resistivity 1–6 × 10^{-3} Ω cm (substrate doping in the 10^{19}–$10^{20}\,\mathrm{cm}^{-3}$ range). Undoped NC samples have been also grown, which show distinct charging mechanisms associated with the passivation of the donor/acceptor NC defect states by substrate free carriers.[14] This issue is quantitatively described in the supplementary material.[15] In particular, it is shown that donor/acceptor defects (with density in the $10^{11} - 10^{13}\,\mathrm{cm}^{-2}$ range) get passivated upon NC doping.[16] They will therefore not be considered hereafter. Three doped NC samples with graded doping level labelled S_1, S_2, and S_3 have been used,[14] and prepared using PH_3 to SiH_4 flow rates of 1/250, 1/50, and 1/25, respectively, and using a constant SiH_4 flow rate of 250 sccm. Fabrication conditions thus lead to nominal *n*-type doping (i.e., atomic density of silicon multiplied by the ratio between PH_3 and SiH_4 flow rates) in the range of ≈10^{20}–$10^{21}\,\mathrm{cm}^{-3}$.[12]

a)Electronic mail: thierry.melin@isen.iemn.univ-lille1.fr

To minimize the influence of surface states associated with the NC native oxide,[17] the NCs and supporting Si substrate have been hydrogen-passivated in a diluted HF solution, rinsed in deionized water, and subsequently loaded in the ultra-high vacuum chamber of an atomic force microscope (VT-AFM, Omicron Nanotechnology) at a base pressure of 10^{-10} mbar. A home-made Amplitude-Modulation KPFM set-up interfaced with a Nanonis controller (SPECS Zürich) has been used to probe the charge state of individual ionized NCs.[18] We used metal-plated cantilever tips (EFM PPP, Nanosensors) with 25 nm apex radius, low-resonance frequency ($f_0 \simeq 70$ kHz) and spring constant ($k \simeq 3$ N m^{-1}). The topography is recorded in non-contact mode with a weak cantilever frequency detuning ($\Delta f = -5$ Hz) corresponding to a 4–5 nm minimum tip-substrate distance during the cantilever oscillation of amplitude ± 15 nm. KPFM data have been recorded simultaneously with the topography, using a $V(t) = V_{dc} + V_{ac}\cos(2\pi f_1 t)$ electrostatic excitation at the cantilever second flexural resonance ($f_1 = 6.2 f_0$, $V_{ac} = 100$ mV). The KPFM signal is the feedback-regulated *dc* bias V_{dc} which nullifies the cantilever oscillation at f_1. Experimental NC KPFM signals are shown in Fig. 1(c) for samples S_1, S_2, and S_3 (data from Ref. 14) as a function of the NC height h. NCs are seen to be positively charged (positive KPFM signal), corresponding to a partial ionization of its dopants. This ionization is generated by the shift of the NC conduction states (and thus, of its Fermi level) upon quantum confinement, leading to an electron transfer from the NCs to the substrate (see the energy diagram and the electron transfer shown in Fig. 1(d)). This mechanism is somehow similar to a remote doping process and is electrostatically limited: an energy equilibrium is set-up when the ionized NC electrostatic energy equals the shift towards higher energies of the NC conduction band upon quantum confinement (energy depicted in red in Fig. 1(d)). The identification of this process has enabled to measure the opening of the NC band-gap upon quantum confinement in Ref. 14.

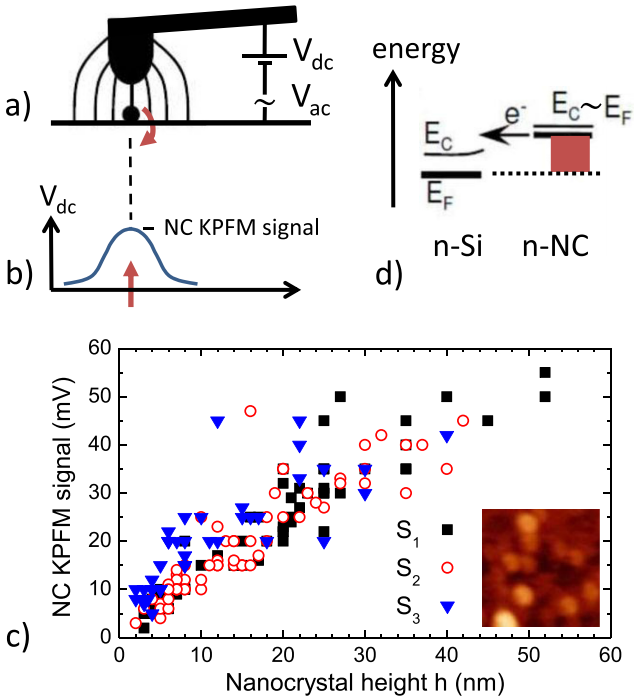

FIG. 1. Schematics of (a) KPFM measurements and (b) KPFM signals over a NC. (c) Experimental NC KPFM signals for samples S_1, S_2, and S_3 as a function of the NC height h (data from Ref. 14). The inset shows a 200 nm topography image of the NCs on the Si substrate. (d) Energy diagram showing the conduction band onsets of the n-doped NC and of the n-doped Si substrate, as well as the charge transfer induced by the NC quantum confinement.

In this work, we go beyond the energy equilibrium considerations, and we focus on extracting the charge states of NCs from experimental KPFM signals. This issue is of particular importance to use doped NCs as electron sources, or to understand transport properties of doped NC arrays. It is also a tedious issue experimentally, since the estimation of the NC charge requires (i) to take into account side-capacitance effects in KPFM experiments[20,21] and their non-linear variations with the tip oscillation at f_0 during KPFM imaging[19] and (ii) to accurately describe the distribution of ionized dopants within the NCs. We will use first a core-charge model (Fig. 2(a)), in which a point charge Q_{core} is located at the NC center, and a junction model assuming randomly distributed dopants (Fig. 2(b)), in which the NC ionized dopants are located at the NC/substrate interface in the form of an abrupt junction of depletion width W and depleted charge Q_{dep}. The core-charge model is obviously adapted to describe experiments in the limit of a full ionization regime (NCs of smaller sizes) while the junction model will be general and enable to quantify the NC depletion width and its actual depletion charge, i.e., the charge transferred from the NC to its environment. A formal link can be drawn between both models since they lead to the same vertical dipole $Q_{core}h/\varepsilon$ (Ref. 22) when used to analyze experimental KPFM data, as sketched in Fig. 2(c) (ε is the NC dielectric constant). Both models are identical in the limit of fully ionized NCs.

Experimental data of Fig. 1 are first analyzed in the framework of the core-charge model. As previously explained, this model is a priori relevant to describe the NC charge in the full-ionization regime but will only provide an "equivalent core-charge value" for partially ionized NCs. We however use this model at first because it will provide a value of the NC doping level N_D from experiments, in the regime of full ionization.

The NC core charge Q_{core} extracted from KPFM data is shown in Fig. 3 as a function of the NC height h. Although the NC electrostatic potential varies over typically one order of magnitude in the 2–50 nm size range due to quantum confinement,[14] the NC charge Q_{core} by comparison only

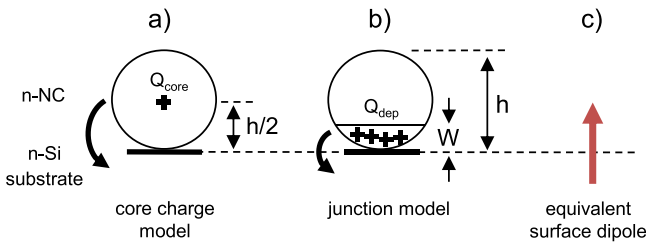

FIG. 2. (a) Core-charge model consisting in a charge Q_{core} located at the NC center; (b) randomly distributed impurity junction model with depletion width W and charge Q_{dep}; (c) equivalent interface dipole $Q_{core}h/\varepsilon$ probed by KPFM (see text).

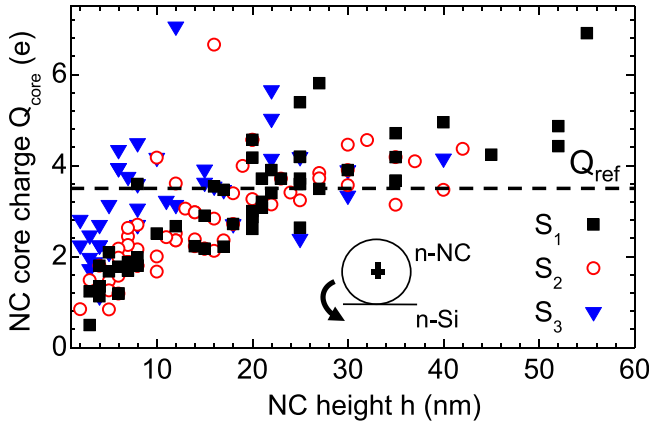

FIG. 3. Plot of the NC charge Q_{core} in the core-charge model for samples S_1, S_2, and S_3. The dotted line corresponds to the average charge value Q_{ref} (see text).

faintly varies with the NC height h, with an average value $Q_{ref} \approx 3.5e$ (dotted line in Fig. 3). This point is striking, and is a signature that electrostatic confinement is enhanced at small NC size, which limits the charge transfer from the NC, in spite of shift of the NC conduction band induced by quantum confinement. The measured value for Q_{core} is the signature of the competition between electrostatic and quantum confinements in the charge transfer equilibrium. The charge transfer equilibrium between the doped NC and substrate can also be viewed, in a first approximation, to the formation of an interface dipole $Q_{ref} \times h/\varepsilon$ linearly increasing with the NC height h, and equal to ≈15 D for $h = 1$ nm. The constant value of Q_{ref} will be later used as a convenient phenomenological parameter to build an analytical model for the NC junction properties in the regime of strong electrostatic and quantum confinements.

To extract the NC doping level N_D from experiments, we define the NC ionized dopant concentration by its charge Q_{core} divided by the NC volume. This quantity accounts for the degree of ionization of the NCs. The NC doping level can then be assessed by looking for its maximum value, i.e., for the regime of full ionization. Data are shown in the supplementary material.[15] The NC ionized dopant concentration $6Q_{core}/\pi h^3$ follows, in the core-charge model, a power-law behaviour $6Q_{core}/\pi h^3 \propto h^{-\alpha}$ with $\alpha = 2.7$ close to 3 and varies over ≈4 orders of magnitude over the size range 2–50 nm. At large NC size, it would predict a low degree of ionization, with a few ionized dopants concentrated at the NC core (see Fig. 3), which is clearly not relevant in a randomly distributed impurity model. At the smallest NC size however, the NCs get fully ionized, and one can use the maximum values for the NC ionized dopant concentration to determine the NC effective doping level for the three samples S_1, S_2, and S_3. The measured doping levels, respectively, reach 8.7×10^{19} cm^{-3}, 2.0×10^{20} cm^{-3}, and 6.7×10^{20} cm^{-3} (NC diameters in the range of 1–3 nm).[15] These doping levels match the graded nominal doping levels expected from growth conditions (i.e., atomic density of silicon multiplied by the ratio between PH_3 and SiH_4 flow rates), in the range of 10^{20} cm^{-3}-10^{21} cm^{-3}. The charge carried by fully ionized NCs is also checked to be consistent with the observation of an elementary charge, as seen from the Q_{core} charge values found between 0 and $2e$ for fully ionized NCs at small NC size.[23]

To provide a reliable view of the charge transferred from the NC beyond the full ionization regime, we analyzed the experimental KPFM data of Fig. 1 in the junction model with depleted charge Q_{dep} and width W (see Fig. 2(b) for a schematics). The calculation was made using the NC doping levels for S_1, S_2, and S_3 previously determined from the core-charge model analysis in the regime of full ionization. Data for Q_{dep} and W are plotted in Fig. 4. It is seen from Fig. 4(a) that the junction depletion width W is remarkably almost independent of the NC diameter for each sample S_1, S_2, and S_3 although some deviations can be observed in the few-charge regime (the shaded areas in Fig. 4(a) indicate the size range in which Q_{dep} is less than 10 elementary charges). This feature is striking since the energy equilibrium ruling the charge transfer varies of ≈one decade in the 2–50 nm NC diameter range due to the quantum effects.[14] The junction depletion width W is also seen to be reduced with larger N_D, as qualitatively expected. We finally analyzed in Fig. 4(b)

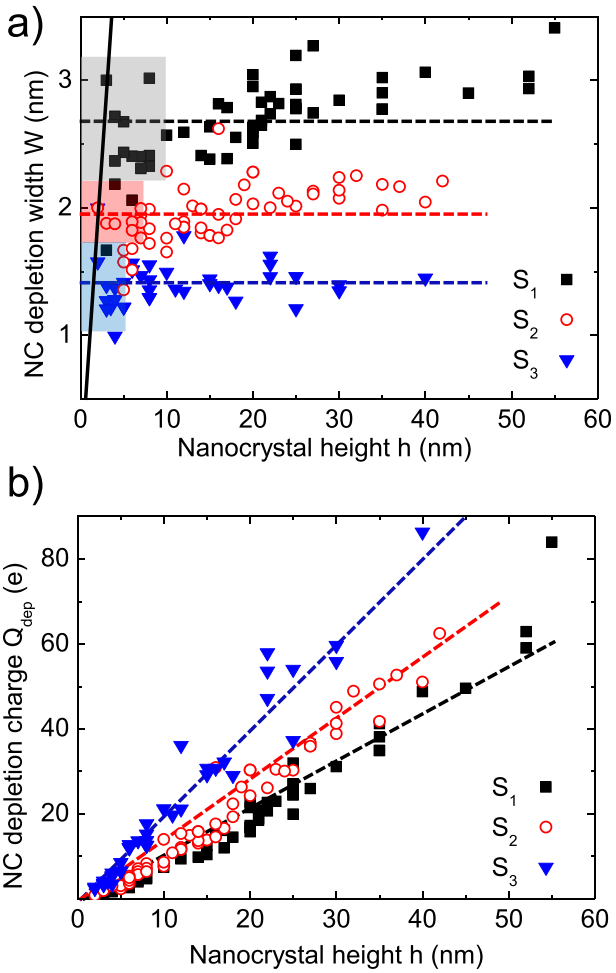

FIG. 4. (a) Junction depletion width W calculated from experimental KPFM data of Fig. 1(c) in the junction model. Data for S_1, S_2, and S_3 have been fitted with a constant value across the 2–50 nm NC diameter range (dotted lines). The coloured shaded areas indicate the size range in which Q_{dep} is less than 10 elementary charges. The solid lines correspond to the full ionization regime limit $W = h$. (b) Junction depletion charge Q_{dep}. Data for S_1, S_2, and S_3 have been fitted linearly as a function of the NC diameter h (dotted lines).

the NC depletion charge Q_{dep}, which varies linearly (dotted lines are linear fits for Q_{dep}), and within typically two decades in the NC size range.

To interpret these data quantitatively, we derive now an analytical model for the junction depletion width W and depletion charge Q_{dep}. The model is phenomenological and based on the formation of a junction corresponding to an interface dipole $Q_{ref}.h/\varepsilon$ proportional to the NC diameter h. It can be easily derived analytically, assuming $W \ll h$.[24] The depleted charge Q_{dep} for a junction of width W and for a doping level N_D is simply related to W and N_D by $Q_{dep}/e = \pi h/2W^2N_D$. One can also similarly calculate the interface dipole generated by the depletion width, which equals $e\pi N_D.(2h/3)W^3/\varepsilon$. We then simply assume that this dipole linearly varies with the NC diameter and equals $Q_{ref}.h/\varepsilon$. In this model, the value of the phenomenological charge Q_{ref} is expected to match the NC charge value obtained in the core-charge model (3) and found in the few e range. The NC depletion width W and depletion charge Q_{dep} can then be expressed as

$$W = \left[\frac{3}{2\pi}\frac{Q_{ref}}{e}\right]^{1/3} \times N_D^{-1/3}, \tag{1}$$

$$\frac{Q_{dep}}{e \times h} = \frac{\pi}{2}\left[\frac{3}{2\pi}\frac{Q_{ref}}{e}\right]^{2/3} \times N_D^{1/3}. \tag{2}$$

These laws for W and Q_{dep} correspond to the constant value of the junction depletion width as a function of the NC diameter and to the linear behaviour of Q as a function of h, as observed in Fig. 4. To test for the validity of the dependence of W and Q as a function of the doping level N_D, we plotted in Fig. 5(a) the average depletion width W for samples S_1, S_2, and S_3 as a function of $N_D^{-1/3}$. The error bars for W correspond to the standard deviation of the values of W in Fig. 4(a) while the error bars on N_D are set to a 30% misaccuracy. The average values for W match the $N_D^{-1/3}$ expectation from Eq. (1). The fitted slope of Fig. 5(a) leads to $Q_{ref} = 3.35 \pm 0.35e$. Similarly, we plotted in Fig. 5(b) the slopes of Q versus h fitted from Fig. 4(b). They exhibit a linear behaviour as a function of $N_D^{1/3}$, which yields a value $Q_{ref} = 3.9 \pm 0.4e$, using Eq. (2). Both values for Q_{ref} coincide within error bars and match the constant value range Q_{ref} observed in the core-charge model (Fig. 3). These results validate the analytical model of Eqs. (1) and (2), which establishes the physical properties of doped nanocrystal semiconductor junctions. The main physical point of the model is the phenomenological charge Q_{ref} (here, $\approx 3.5e$) which describes the interface dipole $Q_{ref} \times h/\varepsilon$ formed by the charge transfer between the NC and substrate, in the regime of strong electrostatic and quantum confinement.

We stress that we here propose an *electrostatic* junction model for the charge transfer between doped NCs and their environment, which, by essence, does not incorporate any quantum effect in itself. The model is analogous in its outputs (depletion width W and depletion charge Q_{dep}) to a conventional *p-n* junction model, in which W and Q_{dep} are calculated from the junction built-in potential. Quantum physics may lay in the value of built-in potential, but not in the electrostatic model which derives W and Q_{dep} from this potential. This point holds as well for our analytical nanocrystal junction model, in which we start from a reference charge Q_{ref} (instead of the junction built-in potential) from which we derive W and Q_{dep}. It is the originality of our paper to propose that a constant reference charge Q_{ref} accounts for both quantum and electrostatic confinements independently of the NC size, and enables analytical predictions of the charge transferred from the NC to its environment. Though the model is in part phenomenological, it brings to the community an analytical tool to predict charge transfers from doped NCs, in the absence of any existing competing model. The use of a constant value of Q_{ref} is not a signature that quantum effects are overlooked, but consists rather in an elegant way to take into account both quantum and electrostatic confinement effects together. The approximation of a constant Q_{ref} value of course corresponds to a value for the junction built-in potential which is enhanced by quantum effects (as evidenced in Ref. 14). The approximation of a constant Q_{ref} value indicates in fact how the enhanced NC junction built-in potential is compensated by the enhanced electrostatic confinement. On a practical basis, it appears simply a convenient tool to describe charge transfers from doped NCs.

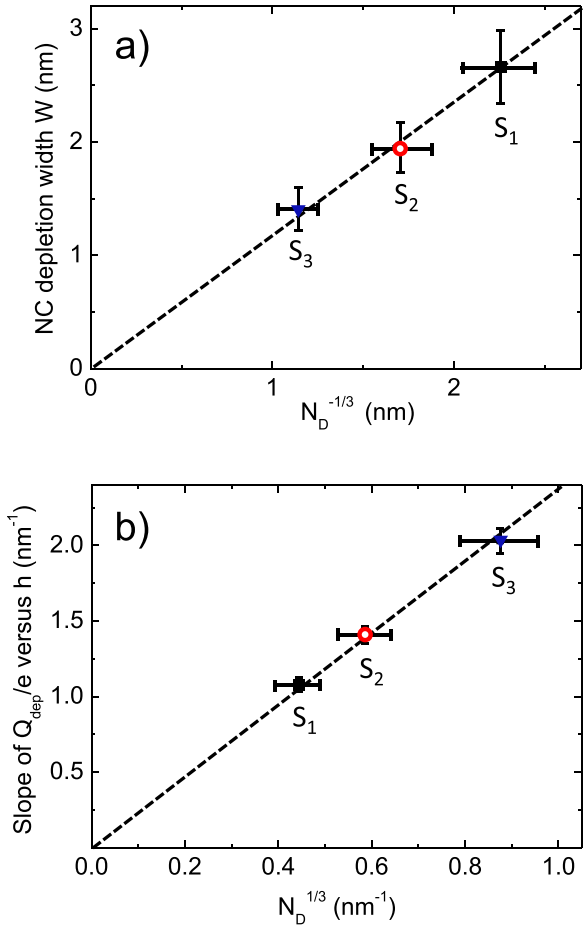

FIG. 5. (a) Average junction depletion width W (dotted lines in Fig. 4(a)) as a function of $N_D^{-1/3}$ for samples S_1, S_2, and S_3. The dotted line is a linear fit, leading to $Q_{ref} = 3.35e \pm 0.35e$ (see text). (b) Linear slope of Q_{dep} versus h in Fig. 4(b), plotted as a function of $N_D^{1/3}$ for samples S_1, S_2, and S_3. The dotted line is a linear fit, leading to $Q_{ref} = 3.9 \pm 0.4e$ (see text).

It should also be pointed out that the observed agreement between the analytical model (using a constant reference charge Q_{ref}) and values for W and Q_{dep} extracted from KFPM experiments falls beyond expectations. In particular, the junction model based on a constant Q_{ref} value nicely agrees with values for W and Q_{dep} extracted from KFPM experiments in Figs. 4 and 5, while Q_{core} values extracted from experimental data (Fig. 3) are not strictly constant and equal to Q_{ref}. Two points explain this feature. First, the analytical model leading to Eqs. (1) and (2) provides expressions for W and Q_{dep} which are power-laws of Q_{ref} with sub-unity exponents. Values of W and Q_{dep} are thus less sensitive to variations of Q_{ref} than the variations of Q_{core} with respect to Q_{ref} observed in Fig. 3. The situation is more complex in the "small" NC size limit (typically, $Q_{dep} \leq 10e$), in which two model limitations are expected: on the one hand, our predictions deal with a continuous junction model while it is compared to experiments in the regime of only a few ionized dopants (see shaded areas in Fig. 4(a), which correspond to a depletion charge Q_{dep} smaller than $10e$). Experimental values for W should therefore expected to become scattered with respect to the model predictions in the small size regime, which explains, in part, the observed fluctuations with respect to a constant W. On the other hand, the model was analytically derived under the assumption of $W \ll h$. A transition is thus expected from a constant value for Q towards the model of full ionization, in which W is simply equal to h. To account for this, we plotted in Fig. 4 the $W = h$ full ionization regime limit as a continuous line. The deviations from a strictly constant W value observed for sample S_1 (lower doped sample) can be seen as a transition towards the regime of full ionization. This point is also consistent with the fact that such deviations are not observed for the higher doped S_3 sample. A model including this transition may be further developed, but our analytical model predicting a constant depletion width W already falls in good agreement with data, within experimental accuracy.

More generally, we infer that this simple model should stay valid for other materials, and more sophisticated homo- or hetero-junctions based on doped semiconductor NCs, with adapted values for Q_{ref}. It should provide an easy tool to describe charge transfers or remote doping properties from doped semiconductor nanocrystals. Our work can hence be used to predict charge transfer densities as a function of the NC doping level and size, e.g., from a linear chain of doped NCs towards a one-dimensional conduction channel, or from a doped NC array towards a two-dimensional conduction channel. Finally, it can be also used to predict local junction electric fields at hand for exciton dissociation in NC-based photovoltaic devices.

In conclusion, we have demonstrated on the basis of KPFM experiments that charge transfers from individual doped NCs towards a two-dimensional layer correspond to the formation of an interface dipole linearly increasing with the NC diameter. We provided an analytical model to predict doped NC junction properties (depletion width and depleted charge) as a function of the NC doping level N_D. This model is the "nanocrystal counterpart" of usual textbook models for semiconductor junctions. It is demonstrated to fall in good agreement with experiments for doped silicon NCs with 2–50 nm sizes and $N_D \approx 10^{20}$–10^{21} cm^{-3}, thus enabling the prediction of charge transfers from doped NCs analytically, and down to quantum size regimes.

ACKNOWLEDGMENTS

The authors acknowledge D. Deresmes, H. Diesinger, M. Zdrojek, C. Delerue, and D. Théron for discussions. This work was supported in part by the French National Research Agency under Contract No. ANR-11-BS10-0004 and using the facilities of the EXCELSIOR Nanoscience Characterization Center.

[1]A. Sahu, M. S. Kang, A. Kompch, C. Notthoff, A. W. Wills, D. Deng, M. Winterer, C. D. Frisbie, and D. J. Norris, Nano Lett. **12**, 2587–2594 (2012).
[2]V. Chikan, Phys. Chem. Lett. **2**, 2783–2789 (2011).
[3]D. J. Norris, A. L. Efros, and S. C. Erwin, Science **319**, 1776–1779 (2008).
[4]See J. A. Smyde and T. D. Krauss, Mater. Today **14**, 382–387 (2011) and references therein.
[5]See, e.g., H. Liu, D. Zhitomirsky, S. Hoogland, J. Tang, I. J. Kramer, Z. Ning, and E. H. Sargent, Appl. Phys. Lett. **101**, 151112 (2012).
[6]See, e.g., U. Banin, Y. Cao, D. Katz, and O. Millo, Nature **400**, 542 (1999).
[7]S. C. Erwin, L. Zu, M. I. Haftel, A. L. Efros, T. A. Kennedy, and D. J. Norris, Nature **436**, 91 (2005).
[8]D. Yu, C. J. Wang, and P. Guyot-Sionnest, Science **300**, 1277 (2003).
[9]S. Ithurria, P. Guyot-Sionnest, B. Mahler, and B. Dubertret, Phys. Rev. Lett. **99**, 265501 (2007).
[10]D. Mocatta, G. Cohen, J. Schattner, O. Millo, E. Rabani, and U. Banin, Science **332**, 77 (2011).
[11]For a recent review, see X. Pi, J. Nanomater. **2012**, 912903 (2012).
[12]A. R. Stegner *et al.*, Phys. Rev. Lett. **100**, 026803 (2008).
[13]See, e.g., P. Roca i Cabarrocas, Th. Nguyen-Tran, Y. Djeridane, A. Abramov, E. Johnson, and G. Patriarche, J. Phys. D: Appl. Phys. **40**, 2258–2266 (2007).
[14]Ł. Borowik, K. Kusiaku, D. Deresmes, D. Théron, H. Diesinger, T. Mélin, T. Nguyen-Tran, and P. Roca i Cabarrocas, Phys. Rev. B **82**, 073302 (2010).
[15]See supplementary material at http://dx.doi.org/10.1063/1.4834516 for a more detailed description about growth conditions of doped silicon nanocrystals, the measurement of the NC charge state from Kelvin probe force microscopy, and the analysis of intrinsic and p–doped NC samples.
[16]This process, however, is not efficient in the case of *p*-type doped NCs grown using trimethylboron as boron source, as due to a lower effective doping and/or enhanced NC defect states (see supplementary material (Ref. 15)).
[17]H. Diesinger, T. Mélin, D. Deresmes, D. Stiévenard, and T. Baron, Appl. Phys. Lett. **85**, 3546 (2004).
[18]See for details H. Diesinger, D. Deresmes, J. P. Nys, and T. Mélin, Ultramicroscopy **110**, 162 (2010).
[19]Ł. Borowik, K. Kusiaku, D. Théron, and T. Mélin, Appl. Phys. Lett. **96**, 103119 (2010).
[20]H. O. Jacobs, P. Leuchtmann, O. J. Homan, and A. Stemmer, J. Appl. Phys. **84**, 1168 (1998).
[21]F. Krok, K. Sajewicz, J. Konior, M. Goryl, P. Piatkowski, and M. Szymonski, Phys. Rev. B **77**, 235427 (2008).
[22]T. Mélin, H. Diesinger, D. Deresmes, and D. Stiévenard, Phys. Rev. Lett. **92**, 166101 (2004).
[23]This core charge in the [0;2 e] range corresponds to single-charged NCs since the dipole associated with an ionized dopant can vary from zero (when located at the substrate interface) to $2eh/\varepsilon$ (when located at the NC top).
[24]This assumption was not made while extracting values of W and Q_{dep} from KPFM experiments in Figs. 4 and 5.